MULTIDISCIPLINARY HYPERSONIC CONFIGURATION OPTIMIZATION

M. Levine, H. Ide, and S. Hollowell
Rockwell International
North American Aircraft
Los Angeles, CA 90009

ABSTRACT

Hypersonic vehicle design involves several complex, highly coupled disciplines. The need to use multidisciplinary optimization techniques to determine the optimal configuration is rather apparent. This paper presents a multidisciplinary configuration optimization technique which directly applies to the very difficult challenge of hypersonic vehicle design.

INTRODUCTION

The developments in computational fluid dynamics (CFD) techniques in recent years are significant. Although CFD analysis can require significant time to be performed due to flow complexity and grid issues, the accuracy with respect to high speed vehicle performance is very reliable. Concurrently, various types of optimization methods based on CFD and CSM (computational structural mechanics) analyses are recieving more attention, references 1-4.

In the case of hypersonic vehicles, the use of multidisciplinary optimization techniques is very important for proper sizing of the vehicle. The key disciplines are aerodynamics, inlet performance, propulsion, and structures. One of the serious concerns in the preliminary design stage is the vehicle performance based on an assumed takeoff gross weight. Particulary, effective specific impulse is an important parameter in the attainment of a desired vehicle trajectory. Since the specific impulse is a direct function of the vehicle thrust and drags, minimizing the drag forces is essential. On the other hand, the same thing can be achieved by maximizing thrust through the improvement of the inlet perfomance and the fuel volumetric efficiency.

The traditional sizing method attains closure on a vehicle design by photographically scaling the baseline to achieve the required fuel fraction. This occurs at the intersection of the fuel required and the fuel available curves,as shown in figure 1. It is possible to attain closure by bringing the fuel required curve down and/or by bringing the fuel available curve up. As a first step, the fuel available will be held constant in the approach in this paper. Hence, the approach in this paper will concentrate on bringing the fuel required curve down. For simplicity, this will be accomplished by maximizing the specific impulse (Isp) at a critical point in the trajectory by modifying the baseline configuration geometry.

In this paper, a specific approach to sensitivity calculation, the determination of independent design parameters, the formation of a global sensitivity matrix, the optimization process, and some results will be shown.

PROBLEM STATEMENT

In order to excercise CFD and other derived sensitivities in an optimization problem, a vehicle specification and a key point in the trajectory are defined. The hypersonic vehicle baseline configuration used in this study is shown in figure 2, including the design variables chosen. Presently, we are dealing only with the forebody of the vehicle for simplicity. Therefore, the effect of the forebody on the aftbody aerodynamics is neglected at this time. The aftbody (ie., nozzle, bodyflap, elevon, etc.) effects are included in the propulsion contributing analysis (CA) and the trim contraint.

The flight condition at which the vehicle will be optimized is as follows; Mach = 16, q = 1500 psf, and α = 0.0 degrees. Finally, the objective function for this optimization is defined as follows.

Objective: maximize I_{sp}

$$I_{sp} = \frac{T - D}{m_f} \tag{1}$$

$$D = \begin{cases} D_0 = D_{ram} + D_{fb} + D_{visc} + D_{aft} \text{ ; UNTRIMMED} & \text{(2a)} \\ D_0 + D_e + D_{bf} \text{ ; TRIMMED} & \text{(2b)} \end{cases}$$

where,

T = thrust
D = drag
m_f = fuel flow rate
D_0 = total untrimmed drag
D_{ram} = ram drag
D_{fb} = forebody pressure drag
D_{visc} = forebody viscous drag
D_{aft} = aftbody drag (held constant)
D_e = elevon drag
D_{bf} = bodyflap drag

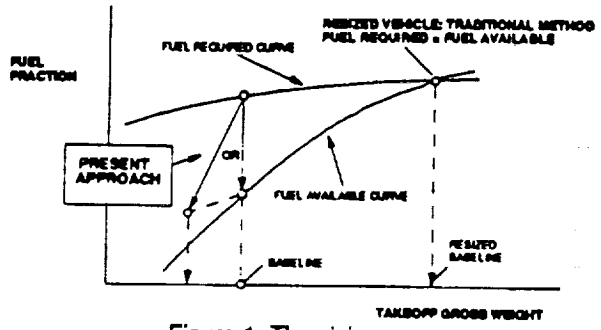

Figure 1. The sizing process

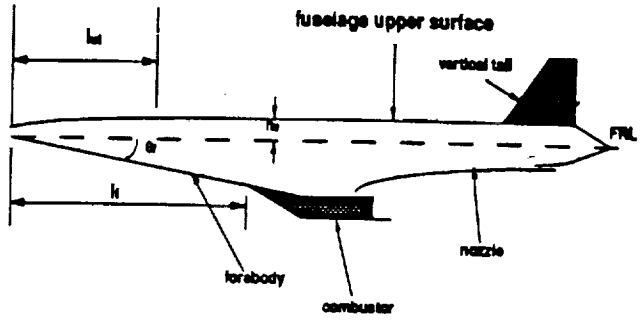

Figure 2. Baseline configuration

OVERALL OPTIMIZATION PROCEDURE

A multidisciplinary decomposition/optimization technique is used to develope the global sensitivities needed by the optimizer in an efficient manner. This technique involves four steps as shown in figure 3. ①Determine the most efficient decomposition of the design process, by identifying the individual contributing analyses (CA's) that makeup the design process using an N-squared diagram. ② Define the linkages between CA's by adding to the N-squared diagram developed in step 1 . ③ Calculate the sensitivity derivatives for each CA independently. ④ Combine the sensitivities in the global sensitivity equations (GSE) to determine the global sensitivity derivatives (GSD) which are then used by the optimizer to determine an optimum configuration. Further background and examples of applications of the methodology can be found in references 5-6. The following sections describe each step in more detail.

1. DECOMPOSE DESIGN PROCESS

The N-squared diagram, shown in figure 4, is a handy tool for presenting the functional decomposition and the linkages between CA's, which are discussed in this and the next section, respectively. It shows some of the disciplines included in the design process.

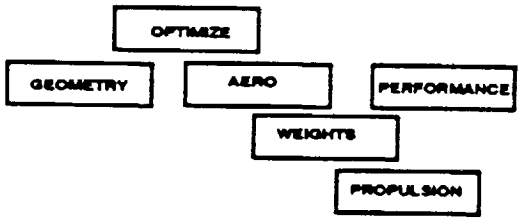

Step 1 - Decompose design process

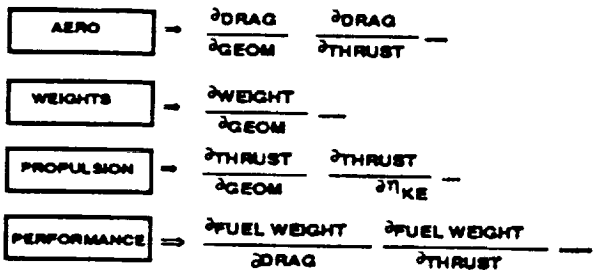

Step 3- Each discipline independently calculate sensitivity derivatives

Each box is a contributing analysis card which contains information about CA. It identifies figures of merit, constraints, and control variables. It also defines the programs to be used to generate the sensitivity data and the person(s) responsible for running them.For the present work, the maximum amount of disciplines used in the results are those shown in figure 5. Results are also presented for optimizations where some of these CA's are not included.

2. DEFINE LINKAGES

Each oval in figure 4 identifies a connection between disciplines. By following the lines away from the oval and towards the CA boxes, the two disciplines involved in the linkage can be identified. Each oval is a data card which identifies the information passed from one CA to another CA. It also defines the person(s) responsible for generating the data and the person(s) that would recieve the data during a traditional design cycle. The linkages that occur in the present work appear as dots in figure 5.

3. CALCULATE LOCAL SENSITIVITY DATA

Each discipline independently calculates the sensitivity derivatives which are defined during step 2. The sensitivity

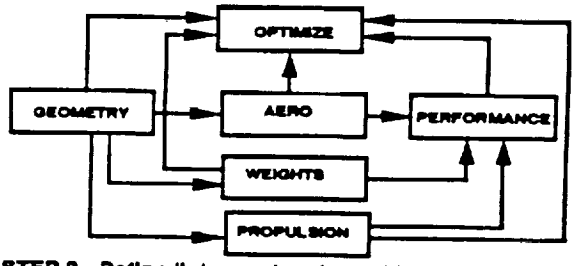

STEP 2 - Define linkages (and sensitivity derivatives)

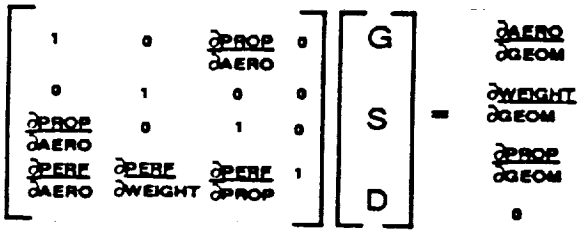

STEP 4 - Solve simultaneous equations for global sensitivity derivatives (GSD) and optimize geometry

Figure 3. Overall optimization procedure

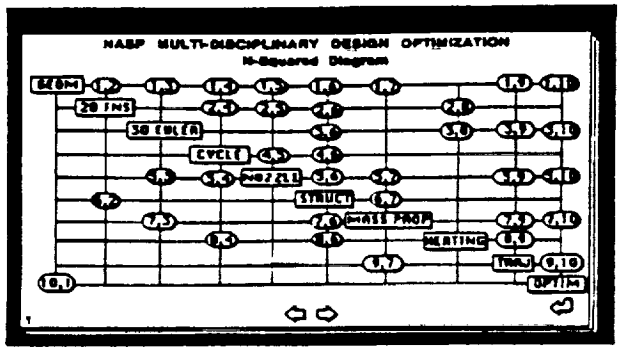

Figure 4. N-squared diagram example

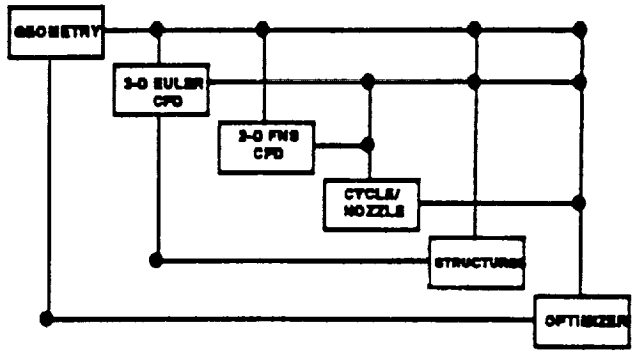

Figure 5. Step 2 for present work

data is calculated using a finite difference approach. Three different ways of determining the sensitivity data and the change in the sensitivity data away from the baseline are presented in figure 6.

The first-order one-sided difference (FO-OSD) approach has the key advantage of requiring only the baseline and one additional run to calculate the first- order sensitivity data. However, the accuracy in the direction opposite to the perturbation can be very poor if the curve is not close to be linear.

The first-order central difference (FO-CD) requires the baseline plus two runs to calculate the sensitivity data. It produces better accuracy than FO-OSD in one direction, but gives up some accuracy in the other direction which makes this approach not worth the extra cost of the additional run.

However, without making any additional runs, than the FO-CD approach, the second-order (SO) approach can be used. The advantage to the SO approach is the ability to model the nonlinearity in the sensitivity data. The FO-OSD approach and the SO approach each have their advantages and disadvantages, which one is best to use depends on the nonlinearity of the problem.

The use of pre/postprocessors in order to speed up the preparation of input data for the aerodynamic and structural flexibilty analysis was very important in generating the local sensitivity data in a timely fashion. The diagram in figure 7 illustrates and describes those used in the present work.

4. SOLVE GLOBAL SENSITIVITY EQUATIONS AND PERORM OPTIMIZATION

The N-squared diagram, in figure 5, translates into the set of global sensitivity equations presented in figure 8. Any of the disciplines shown can be neglected by removing the proper rows and columns from the matrix equation. For example, in order to remove the effect of the 2-D Navier-Stokes CA from the optimization, the first row and first column would be deleted.

The right-hand side (RHS) of the equation deals with the local sensitivity of the outputs from each CA with respect to a single design variable. If the design variable is not a direct input to a particular CA, then all the local sensitivities in the RHS are zero with respect to that variable for that CA as shown in figure 8 for the propulsion CA.

The left-hand side (LHS) includes the cross-coupling (or linkage) sensitivity matrix and the solution vector. The

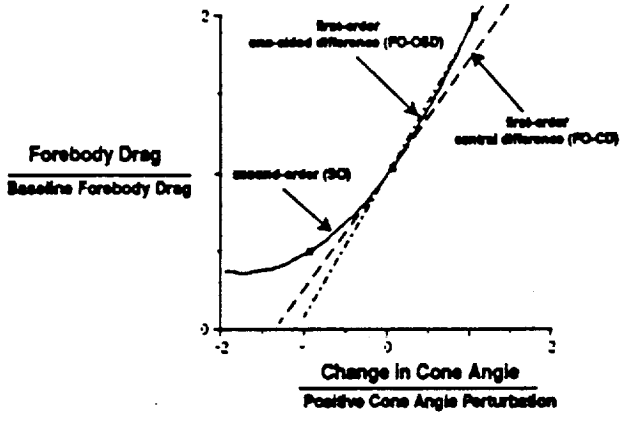

Figure 6. Sensitivity calculation

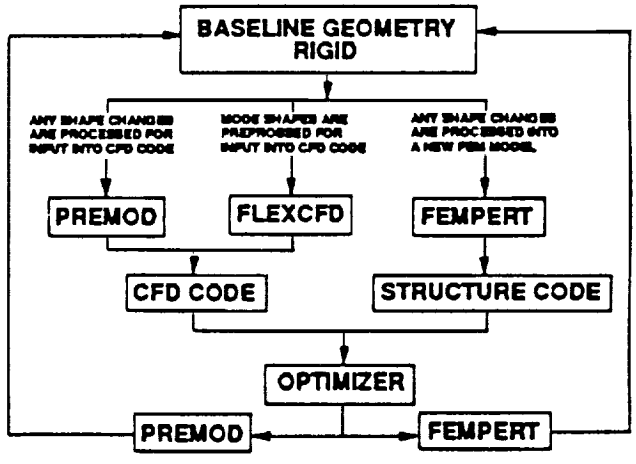

Figure 7. Pre/postprocessors

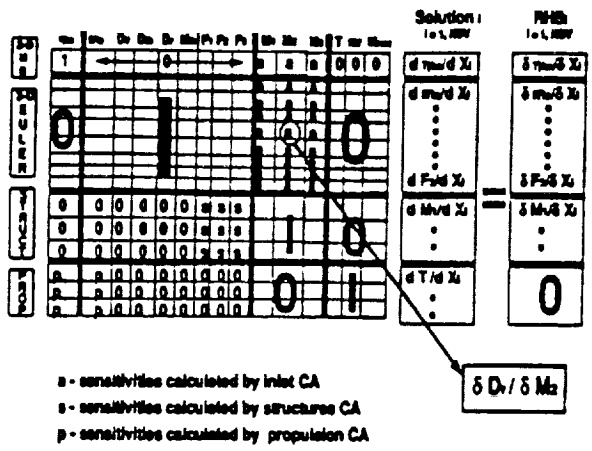

Figure 8. Global sensitivity equations

solution vector contains the global sensitivity of the outputs from each CA with respect to a single design variable. There will be one RHS and one solution vector for each design variable. It is important to note that although the local sensitivities on the RHS are zero for a particular CA with respect to a particular design variable the global sensitivities need not be zero.

The resulting global sensitivity data is then used to update the vehicle performance during the optimization run. This is accomplished using a Taylor series expansion for each of the outputs from each of the CA's. The objective function and the constraints are then updated and passed to the optimizer.

The optimizer used in the present work is the ADS (Automated Design Synthesis) program, reference 7, with ISTRAT=0, IOPT=4, and IONED=7. ISTRAT=0 indicates that no initial strategey is used. The use of the Method of Feasible Directions (MFD) for constrained minimization, references 8-9, is indicated by IOPT=4. The one-dimensional search, IONED=7, finds the minimum of an constrained function by first finding bounds and then using polynomial interpolation.

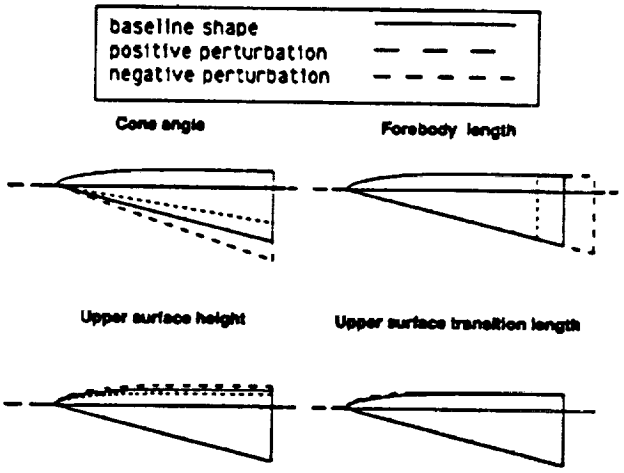

Figure 9. Design variables

CONFIGURATION DECOMPOSITION

The configuration is decomposed into independent design variables which are used by the optimizer to improve the vehicle performance. The design variables which will be used in the hypersonic forebody optimization example in this paper are shown in figure 9. The main concern when decomposing a configuration is to make the design parameters ass independent as possible. The more independent they are the larger the allowable move limit in the optimization run, which can possibly reduce the number of optimization cycles. At the beginning of each cycle, the final shape from the previous cycle is analyzed and new global sensitivities are generated. By reducing the number of optimization cycles, a substantial amount of computational cost and time can be saved.

RESULTS AND DISCUSSION

In this paper, four optimization cases are examined. The objective function for the first two cases uses equation 2a in conjunction with equation 1. These equations produce an untrimmed specific impulse (Isp). Cases 3 and 4 use equation 2b instead of 2a to produce a trimmed Isp for the objective function. All four cases have a forebody tank volume constraint for simplicity and to concentrate on one aspect of the present approach's capability. The design variables are limited to a maximum of 10% change, plus or minus, from the baseline values. Each case adds either another CA or an additional constraint to the optimization process. More details and results of each case are discussed in the following paragraphs.

CASE 1

The initial optimization case shown in this paper contains the CA's, 3-D Euler and propulsion. As a first step, the objective is to maximize an untrimmed Isp, neglecting viscous effects on inlet performance, trim effects, and flexibility effects. These additional effects will be added one at a time into the cases to follow. The only constraint for this case is the forebody tank volume constraint, which is defined as follows:

$$-\varepsilon < (\text{present tank volume} - \text{baseline tank volume}) < \varepsilon \quad (3)$$

$$\varepsilon = 0.1\ \%\ \text{of the baseline tank volume}$$

The results of case 1 are shown in figure 10. The most significant design variable change occurs to the geometric transition length (DV-4). The increase in this design variable decreases the tank volume slightly, but it significantly decreases the forebody drag which is a key factor in maximizing the Isp. The loss in volume is compensated by the other varaibles. The forebody length (DV-1) increases while the cone angle (DV-2) decreases to produce a more slender forebody which helps maintain the tank volume while reducing the drag. The upper surface height (DV-3) paramater is relatively ineffective, although it increases slighty to help maintain the tank volume. The optimizer predicts approximately a 17% increase in the untrimmed effective Isp.

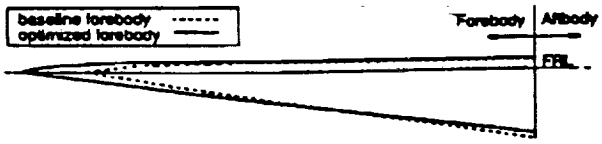

Optimization Parameter	Optimization Results *
Design Variable	
1 - Forebody length	1.0562
2 - Cone angle	0.9067
3 - Upper surface height	1.0126
4 - Geometric transition length	1.1000
Objective	
Effective Isp	1.1693

* Normalized by baseline values, baseline effective Isp is untrimmed

Figure 10. Case 1 results - initial optimization

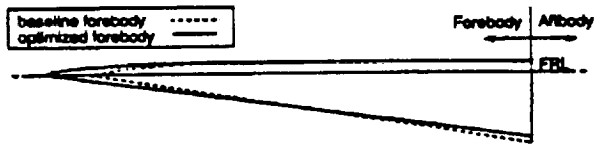

Optimization Parameter	Optimization Results *
Design Variable	
1 - Forebody length	1.0375
2 - Cone angle	0.9367
3 - Upper surface height	1.0153
4 - Geometric transition length	1.1000
Objective	
Effective Isp	1.1681

* Normalized by baseline values, baseline effective Isp is untrimmed

Figure 11. Case 2 results - addition of 2-D Navier-Stokes contributing analysis to case 1

CASE 2

The second optimization case is the same as case 1 with the addition of the 2-D Navier-Stokes CA. This CA contributes the viscous effects on inlet performance to the optimization process.

The results for case 2 show that the changes in the design variables are qualitatively similar to case 1, as shown in figures 10-11. DV-3 and DV-4 have almost identical changes in magnitude in cases 1 and 2, which is due to the fact that these two variables have an insignificant effect on inlet performance. However, the magnitude of the changes in DV-1 and DV-2 are smaller for case 2. This indicates that the benefits of making the forebody more slender reaches a maximum closer to the baseline shape when the viscous effects on the inlet performance are included in the process. Even with these differences in magnitude, the objective function value is almost identical in the two cases. This is due to a positive viscous effect on the inlet performace due to the change in DV-1 and -2, which counter-balances the increase in drag for the less slender forebody.

CASE 3

The third optimization case uses equations 1 and 2b to produce a trimmed Isp for the objective function. It includes the same CA's as case 2 with an added constraint. The constraint added is for maintaining trim given a trimmed baseline vehicle, and it is defined as follows:

$$-\varepsilon < (\text{summation of changes in moments}) < \varepsilon \qquad (4)$$

ε = 1 % of the baseline summation of moments

In order to trim the vehicle, the elevon deflection (DV-5) and the bodyflap deflection (DV-6) must be included as design variables. For this paper, these control surfaces produce only a moment and a drag. For simplicity, the effect of the bodyflap on the propulsion is neglected. The moments are used to satisfy equation 4, and the drags, which appear in equation 2b, are the performance penalty for trimming the vehicle. In order to start the optimization, a baseline condition for the control surfaces is required. The baseline condition for this paper is a 5.0 degrees deflection for both surfaces. These deflections add drag to the baseline, which creates a lower baseline Isp than the untrimmed cases.

The changes in DV-1 through -4 are similar to case 2, as shown in figure 12. It is important to note that the 20 % increase in the objective function is with respect to a trimmed baseline Isp. The percent changes in the previous cases are with respect to an untrimmed baseline Isp, which is larger than the trimmed value due to not including the drag from the control surfaces. Therefore, the actual value of the objective may be larger for case 2 than it is for case

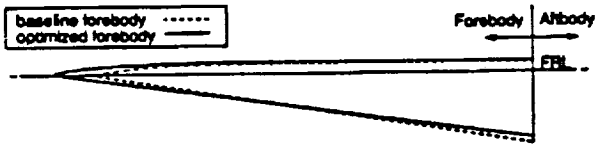

Optimization Parameter	Optimization Results *
Design Variable	
1 - Forebody length	1.0339
2 - Cone angle	0.9480
3 - Upper surface height	1.0095
4 - Geometric transition length	1.1000
5 - Elevon deflection	0.6820
6 - Bodyflap deflection	1.0020
Objective	
Effective trimmed Isp	1.2053

* Normalized by baseline values, baseline effective Isp is trimmed

Figure 12. Case 3 results - addition of trim constraint to case 2

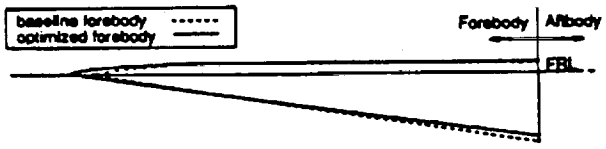

Optimization Parameter	Optimization Results *
Design Variable	
1 - Forebody length	1.0209
2 - Cone angle	0.9693
3 - Upper surface height	1.0029
4 - Geometric transition length	1.0760
5 - Elevon deflection	0.8620
6 - Bodyflap deflection	1.0320
Objective	
Effective trimmed Isp	1.1258

* Normalized by baseline values, baseline effective Isp is trimmed

Figure 13. Case 4 results - addition of flexibility to case 3

3. Of the two additional variables only the bodyflap seems to be effective. The optimized shape actually requires less bodyflap deflection than the baseline which reduces the drag due to this control surface. This accounts for most of the increase in the percentage change in the objective.

CASE 4

The fourth optimization case is the same as case 3 with the addition of the structures CA. This CA contributes the forebody flexibility effect to the optimization process. For simplicity, the structural flexibility CA is only linked to the 3-D Euler CA, and it is not presently linked to the 2-D Navier-Stokes CA,as seen in figure 5. Hence, the effect of flexibility on the viscous part of the inlet flow is neglected. The procedure for adding structural flexibility to the optimization process is described in more detail in reference 6.

In the previous cases, the optimizer produced a longer and more slender forebody. By adding the flexibility effect into the optimization process, the same type of shape occured, except that the design variables remained closer to the baseline values, as seen in figure 13. This indicates that the benefits of making the forebody longer and more slender reaches a maximum closer to the baseline shape when the flexibility effects on the forebody aerodynamics and the inviscid inlet performance are included in the process. For a rigid vehicle when the optimizer increases the forebody length and decreases the cone angle, the forebody drag is reduced. However, for a flexible vehicle these changes also generate larger deflections due to the air loads, which produces more drag compared to treating the vehicle as rigid. Eventually, the optimizer reaches a point where an additional increase in DV-1 and a decrease in DV-2 creates more additional drag due to flexibility than the decrease in drag due to the design variable changes. This explains why the change in the design variables and the improvement in the trimmed specific impulse is much smaller in case 4 than it is in case 3.

CONCLUDING REMARKS

A multidisciplinary configuration optimization technique which directly applies to the very difficult challenge of hypersonic vehicle design is presented and demonstrated. A simple hypersonic forebody design problem is used as an application of the technique. The basic result of the four optimizations is that a longer and more slender forebody produced a higher specific impulse. It is interesting to note that qualitatively the changes in the forebody design parameters are similar for all four cases.

By adding the 2-D Navier-Stokes CA to the initial optimization case, it is discovered that the inlet performance increased from viscous effects due to the design variable changes. However, this positive effect dropped off as the design varaibles got farther away from the baseline, which is evident from the case 2 results.

The most interesting result of adding the trim constraint is that the forebody shape changes (DV-1 through - 4) are almost identical to the previous case. In addition, the shape changes actually required trim moment from the control surfaces, which also reduced the trim drag. For the problem presented, only the bodyflap was effective in maintaining the trim constraint.

The result of adding the flexibilty is the same as result in reference 6. The addition of the other disciplines had no qualitative effect on the structural effect on the optimization results.

Future work will investigate optimizing for multiple design points. This can be accomplished by adding the trajectory contributing analysis. In addition, the optimization of the rest of the vehicle's shape (ie., aftbody, wing, inlet, etc.) needs to be included in the process.

REFERENCES

1. Abdi, F. F., Ide, H., and Shankar, V. J., "Optimization of Nonlinear Aeroelastic Tailloring Criteria," ICAS-88-5.7.3, 16th ICAS Conference, Jerusalem, Israel, 1988.

2. Ide, H., Abdi, F. F., and Shankar, V. J., "CFD Sensitiiv-ity Study for Aerodynamic/Control Optimization Problems," AIAA Paper No. 89-2336, 29th SDM Conference, Wil-liamsburg, VA, April 1988.

3. Ide, H. and Levine, M. S., "Use of Second-Order CFD Generated Global Sensitivity Derivatives for Coupled Problems," AIAA Paper No. 89-1178, 30th SDM Confer-ence, Mobille, AL, April 3-5, 1989.

4. Giles, G. L., Tatum, K. E., and Foss, W. E., "Effects of Nonlinear Aerodynamics and Static Aeroelasticity on Mission Performace Calculations for a Fighter Aircraft," presented at Second NASA/Air Force Symposium on Recent Advances in Multidisciplinary Analysis and Optimi-zation, Hampton, VA, September 1988.

5. Sobieski, J. S., "On the Sensitivity of Complex, Inter-nally Coupled Systems," AIAA Journal, January 1990.

6. Abdi, F. F., Ide, H., Levine, M. S., and Austel, L., "The Art of Aerospace Design: A Multidisciplinary Challenge," presented at Second NASA/Air Force Symposium on Recent Advances in Multidisciplinary Analysis and Optimization, Hampton, VA, September 1988.

7. Vanderplaats, G. N., Sugimoto, H., and Sprague, C. M., "ADS-1: A New General-Purpose Optimization Pro-gram," AIAA Journal, Vol. 22, No. 10, October 1984.

8. Zoutendijk, M., Methods of Feasible Directions, Elsevier Publishing Co., Amsterdam, 1960.

9. Vanderplaats, G. N., and Moses, F., "Structural Optimization by Methods of Feasible Directions," Journal of Computers and Structures, Vol. 3, Pergamon Press, July 1973, pp. 739-755.